Atmos. Chem. Phys. Discuss., https://doi.org/10.5194/acp-2018-716
Manuscript under review for journal Atmos. Chem. Phys.
Discussion started: 5 December 2018

Trends in Global Tropospheric Ozone Inferred from a Composite Record of TOMS/OMI/MLS/OMPS Satellite Measurements and the MERRA-2 GMI Simulation

Jerry R. Ziemke[1,2], Luke D. Oman[1], Sarah A. Strode[1,4], Anne R. Douglass[1], Mark A. Olsen[1,2], Richard D. McPeters[1], Pawan K. Bhartia[1], Lucien Froidevaux[3], Gordon J. Labow[5], Jacquie C. Witte[5], Anne M. Thompson[1], David P. Haffner[5], Natalya A. Kramarova[1], Stacey M. Frith[5], Liang-Kang Huang[5], Glen R. Jaross[1], Colin J. Seftor[5], Mathew T. Deland[5], Steven L. Taylor[5]

[1]NASA Goddard Space Flight Center, Greenbelt, Maryland, USA
[2]Morgan State University, Baltimore, Maryland, USA
[3]NASA Jet Propulsion Laboratory, California, USA
[4]Universities Space Research Association, Columbia, MD, USA
[5]SSAI, Lanham, Maryland, USA

Abstract. Past studies have suggested that ozone in the troposphere has increased globally throughout much of the 20th century due to increases in anthropogenic emissions and transport. We show by combining satellite measurements with a chemical transport model that during the last four decades tropospheric ozone does indeed indicate increases that are global in nature, yet still highly regional. Satellite ozone measurements from Nimbus-7 and Earth Probe Total Ozone Mapping Spectrometer (TOMS) are merged with ozone measurements from Aura Ozone Monitoring Instrument/Microwave Limb Sounder (OMI/MLS) to determine trends in tropospheric ozone for 1979-2016. Both TOMS (1979-2005) and OMI/MLS (2005-2016) depict large increases in tropospheric ozone from the Near East to India/East Asia and further eastward over the Pacific Ocean. The 38-year merged satellite record shows total net change over this region of about +6 to +7 Dobson Units (DU) (i.e., ~15-20% of average background ozone), with the largest increase (~4 DU) occurring during the 2005-2016 Aura period. The Global Modeling Initiative (GMI) chemical transport model with time-varying emissions is included to evaluate tropospheric ozone trends for 1980-2016. The GMI simulation for the combined record also

depicts greatest increases of +6 to +7 DU over India/east Asia, identical to the satellite measurements. In regions of significant increases in TCO the trends are a factor of 2-2.5 larger for the Aura record when compared to the earlier TOMS record; for India/east Asia the trends in TCO for both GMI and satellite measurements are ~+3 DU-decade^{-1} or greater during 2005-2016 compared to about +1.2 to +1.4 DU-decade^{-1} for 1979-2016. The GMI simulation and satellite data also reveal a tropospheric ozone increase of ~+4 to +5 DU for the 38-year record over central Africa and the tropical Atlantic Ocean. Both the GMI simulation and satellite-measured tropospheric ozone during the latter Aura time period show increases of ~+3 DU-decade^{-1} over the NH Atlantic and NE Pacific.

1. Introduction

Over the last several decades there have been substantial regional changes in global pollutants including precursors of tropospheric ozone as documented by many studies (e.g., Granier et al., 2011; Parrish et al., 2013; Cooper et al., 2014; Lee et al., 2014; Zhang et al., 2016; Heue et al., 2016; Lin et al., 2017). The largest increases in global pollutants over the last four decades occurred broadly over a region extending from the Near East to India and east/SE Asia. Lin et al. (2017) used a global chemistry-climate model (CCM) for 1980-2014 to study the effects of global changes in emissions on surface ozone. They show that rising increases in emissions, including a tripling of Asian NO_x ($NO + NO_2$) since just 1990, lead to large increases in surface ozone over India/East Asia and to a lesser extent over the western US due to long-range transport. Shepherd et al. (2014, and references therein) suggest that increases in global tropospheric ozone have occurred during much or most of the 20th century due to increases in anthropogenic emissions. The model simulation by Shepherd et al. (2014) indicates (their Figure 5) positive trends in global tropospheric ozone since 1960, primarily in the tropics and NH extra-tropics.

The changes in global emissions since 1980 are described by Zhang et al. (2016) as an equatorward redistribution over time into developing countries of India and those of SE Asia. Zhang et al. (2016) used a global chemical-transport model (CTM) for 1980-2010 to quantify the effects on tropospheric ozone from these changes in emissions. The model simulations and

Atmos. Chem. Phys. Discuss., https://doi.org/10.5194/acp-2018-716
Manuscript under review for journal Atmos. Chem. Phys.
Discussion started: 5 December 2018

Atmospheric Chemistry and Physics Discussions

OMI/MLS satellite measurements employed by Zhang et al. (2016) indicated largest increases in tropospheric ozone extending from the Near East to India and SE Asia and further eastward over the Pacific Ocean. Zhang et al. (2016) included IAGOS aircraft ozone profiles that also showed large increases (i.e., double-digit percent increases) for India, SE Asia, and East Asia between the 1994-2004 and 2005-2014 time records. The model used by Zhang et al. (2016) also simulated a net increase in global tropospheric ozone of about 28 Tg (~8.9%) over the 30-year record. The results by Zhang et al. (2016) appear consistent with the Bulletin of the American Meteorological Society BAMS State of the Climate Report for year 2016 that indicates about 21.8 Tg increase in OMI/MLS tropospheric ozone when averaged over 60^{o}S-60^{o}N between October 2004 and December 2016, with largest contribution to global trends (about +3 to +4 DU-decade^{-1} for OMI/MLS) originating from the same India and east/SE Asia region. The first evidence of increases in tropospheric ozone over SE Asia from satellite data was shown by Beig and Singh (2007). Beig and Singh used a version of Convective-Cloud Differential (CCD) gridded tropospheric ozone for 1979-2005 that was a predecessor to the current CCD data used for our study (discussed in Section 2). The CCD algorithm is described by Ziemke et al. (1998). The largest increases in tropospheric ozone reported by Beig and Singh (2007) were up to 7-9% decade^{-1} and were located in SE Asia.

Gaudel et al. (2018) (i.e., Chapter 6 of the international Tropospheric Ozone Assessment Report, TOAR) provides analyses of trends in tropospheric ozone calculated from a large array of data sources including satellite, aircraft, balloon ozonesondes and surface measurements. Figure 24 of Gaudel et al., (2018) shows calculated linear trends/decadal changes during the Aura time record for six global data products, five from satellite and one from trajectory-mapped ozonesondes. The six products show large divergence in estimated trends, in part due to their short and differing time records; it was noted that one should be careful about placing precise numbers on estimated trends in TCO from the results. Figure 25 of Gaudel et al. (2018) combined all six TCO products together statistically and showed that the largest and most consistent (and positive) trends between the six products were centered over SE Asia.

Heue et al. (2016) derived a merged 1995-2015 tropical tropospheric ozone dataset from multiple satellite instruments using a variant of the CCD approach for latitude range ±20^o. Their dataset

Atmos. Chem. Phys. Discuss., https://doi.org/10.5194/acp-2018-716
Manuscript under review for journal Atmos. Chem. Phys.
Discussion started: 5 December 2018

Atmospheric Chemistry and Physics
Discussions

was determined by concatenating measurements from several instruments including SCIAMACHY and GOME (but not including either TOMS or OMI/MLS). Their main findings included evidence for increases in tropospheric ozone over both India/SE Asia and the tropical Africa/Atlantic region; however, their largest detected positive trends were across tropical Africa/Atlantic rather than India/SE Asia. Heue et al. (2016) estimated a mean trend in TCO of about +0.7 DU-decade^{-1} in the tropics (15°S-15°N). Leventidou et al. (2018) using similar (but processed differently) SCIAMACHY/GOME CCD TCO measurements for 1995-2015 found ~+3 DU-decade^{-1} trend over southern Africa, but no statistical change in the tropics (15°S-15°N).

The purpose of our study is to derive trends in tropospheric ozone for 1979-2016 by combining TOMS (1979-2005) and OMI/MLS (2005-2016) measurements. A main incentive is to evaluate TCO trends for a longer satellite record than previous investigations including TOAR, and to identify and possibly explain the regional trend patterns that emerge from the data. Areal coverage for calculated trends is all longitudes and latitudes 30°S – 30°N for TOMS and 60°S-60°N for OMI/MLS. The Global Modeling Initiative (GMI) chemical transport model (CTM) replay simulation is included to assess ozone trends during both the TOMS and OMI/MLS time periods. All satellite ozone products were re-processed from previous versions to improve data quality for trend calculations. We also provide a preliminary evaluation of tropospheric column ozone (TCO) measured from the Ozone Mapping Profiler Suite (OMPS) nadir-mapper and limb-profiler instruments beginning in 2012 as possible future continuation of the OMI/MLS TCO record. Section 2 discusses the satellite measurements, GMI model, ozonesonde data, and trend calculations. Section 3 discusses derived trends in tropospheric ozone including net changes for the combined 38-year record. Results are summarized in Section 4.

2. Satellite Measurements, MERRA-2 GMI Model, Ozonesondes, and Trend Calculations.

2.1. Satellite Measurements.

All satellite measurements of TCO used for our study are developed within NASA Goddard Code 614 and updated and upgraded periodically for the science community. TCO measurements and their validation from Nimbus-7 (N7) and Earth Probe (EP) TOMS instruments are discussed by Ziemke et al. (2005, and references therein). TOMS TCO for 1979-2005 is derived using the Convective-Cloud Differential (CCD) algorithm (Ziemke et al., 1998) which differences clear versus thick cloud measurements of column ozone. Useful CCD gridded TCO is limited mostly to tropical latitudes. Our TOMS CCD dataset originates from a preliminary TOMS CCD gridded dataset that Beig and Singh (2007) used for evaluating TCO trends, but now includes a re-processing with extensive flagging of outliers out to latitudes ±30^o. The N7 and EP TOMS instruments have similar spectral/spatial/temporal resolution with TCO obtained from both using the same version 8 algorithm. TOMS TCO is determined by subtracting thick cloud column ozone measurements (to estimate stratospheric column ozone, SCO) from near clear-sky total column ozone. By differencing SCO and total ozone from the same instrument, derived TCO is largely self-calibrating over time and should not be affected by instrument/inter-instrument drifts or offsets. Standard precision error (i.e., 1σ standard deviation) of TOMS gridded TCO is estimated to be about 1.7 DU (e.g., Ziemke et al., 1998).

We also include OMI/MLS TCO (Ziemke et al., 2006) for January 2005-December 2016 and latitude range 60^{o}S-60^{o}N. TCO is determined by subtracting MLS SCO from OMI total column ozone each day at each grid point. Tropopause pressure used to determine SCO invoked the WMO 2K-km^{-1} lapse-rate definition from NCEP re-analyses. For consistency these same lapse-rate tropopause pressure fields were used to derive TCO for ozonesondes, OMPS, and the GMI model (discussed below). OMI total column ozone is retrieved using the OMTO3 v8.5 algorithm that includes in situ UV cloud pressures from OMI (Vasilkov et al., 2008) and several other improvements from version 8. The OMI total ozone and cloud data including discussion of data quality are available from https://ozoneaq.gsfc.nasa.gov/. The MLS data used to obtain SCO were derived from their v4.2 ozone profiles (https://mls.jpl.nasa.gov/data/datadocs.php/). We estimate 1σ precision for the OMI/MLS monthly-mean gridded TCO product to be about 1.3 DU. The additional Supporting Material discusses both validation and adjustments made to OMI/MLS TCO. It can be shown that OMI/MLS TCO derived from this residual technique is nearly identical to the TCO from OMI CCD measurements for the same time period, albeit with the CCD data limited mostly to tropical/subtropical latitudes (e.g., Ziemke et al., 2012).

Atmos. Chem. Phys. Discuss., https://doi.org/10.5194/acp-2018-716
Manuscript under review for journal Atmos. Chem. Phys.
Discussion started: 5 December 2018

Tropospheric ozone for January 2012 through 2016 is also determined from the OMPS nadir-mapper and limb-profiler instruments onboard the National Polar-orbiting Operational Environmental Satellite System (NPP) spacecraft. The OMPS tropospheric ozone is evaluated for possibly continuing the OMI/MLS data record. TCO is determined by subtracting OMPS v2.5 limb-profiler SCO from OMPS v2.3 nadir-mapper total column ozone. SCO is determined from the limb-profiler measurements using the same tropopause pressure fields as for MLS SCO. With both OMPS instruments onboard the same NPP satellite, the time difference between the limb and nadir measurements is about 7 minutes (similar to Aura MLS and OMI instruments). The OMPS data including evaluation of data quality are available from https://ozoneaq.gsfc.nasa.gov/data/omps/.

All satellite-derived TCO represents monthly-means under mostly clear-sky conditions with radiative cloud fractions < 40%. This cloud threshold reduces the number of total column ozone pixels by ~20%. The cloud filtering was applied to reduce precision error in satellite-measured TCO due to errors in assumed climatological below-cloud ozone for thick cloud scenes. These errors in tropospheric ozone are largely random in nature on a pixel-by-pixel basis and do not affect calculated trend magnitudes whether or not such measurements are removed from the analyses. Satellite-derived TCO was gridded to $5^o \times 5^o$ bins centered on longitudes -177.5^o, -172.5^o, …, 177.5^o, and latitudes -27.5^o, -22.5^o, …, 27.5^o for TOMS and latitudes -57.5^o, -52.5^o, …, 57.5^o for OMI/MLS (and also OMPS). This bin size for all measurements was chosen for consistency because the original bin size for the CCD measurements for 1979-2005 is $5^o \times 5^o$.

2.2. MERRA-2 GMI Model.

The Modern-Era Retrospective analysis for Research and Applications (MERRA-2) GMI simulation is produced with the Goddard Earth Observing System (GEOS) modeling framework (*Molod et al*., 2015), using winds, temperature, and pressure from the MERRA-2 reanalysis (*Gelaro et al*., 2017). The configuration for this study is a dynamically constrained replay (*Orbe et al*., 2017) coupled to the Global Modeling Initiative's (GMI) stratospheric and tropospheric chemical mechanism (*Duncan et al*., 2007; *Oman et al*., 2013; *Nielsen et al*., 2017). The simulation was run at ~0.5° horizontal resolution, c180 on the cubed sphere, and output on the same 0.625° longitude x 0.5° latitude grid as MERRA-2 from 1980-2016.

Atmos. Chem. Phys. Discuss., https://doi.org/10.5194/acp-2018-716
Manuscript under review for journal Atmos. Chem. Phys.
Discussion started: 5 December 2018

The MERRA-2 GMI simulation includes emissions of NO, CO, and other non-methane hydrocarbons from fossil fuel and biofuel sources, biomass burning, and biogenic sources. There are also NO emissions from lightning and soil. Fossil fuel and biofuel sources are prescribed from the MACCity Measuring Atmospheric Composition and Climate megaCity – zoom for the environment (MACCity) inventory (*Granier et al*, 2011), which interpolates to each year from the decadal Atmospheric Chemistry and Climate - Model Inter-comparison Project (ACCMIP) emissions (*Lamarque et al*, 2010) and applies a seasonal scaling factor. The MACCity inventory ends in 2010, so for later years we use fossil fuel and biofuel emissions from the Representative Concentration Pathways 8.5 (RCP8.5) scenario. Time-dependent biomass burning emissions for 1997 onwards come from the Global Fire Emissions Dataset (GFED) version 4s (*Giglio et al.*, 2013). Biomass burning emissions for prior years have interannual variability from regional scaling factors based on the TOMS aerosol index (*Duncan et al*, 2003) imposed on a climatology derived from GFED-4s, similar to the approach used in *Strode et al.* [2015]. Emissions of isoprene and other biogenic compounds are calculated online using the Model of Emissions of Gases and Aerosols from Nature (MEGAN) model [*Guenther et al.*, 1999, 2000], and thus respond to MERRA-2 GMI meteorology. NO emissions from soil, parameterized based on *Yienger and Levy* [1995], also responds to the MERRA-2 meteorology. Lightning NO production is prescribed monthly based on the scheme described in *Allen et al*. (2010) using a de-trended cumulative mass flux in the mid-troposphere from MERRA-2, constrained seasonally with the OTDLIS v2.3 climatology (*Cecil et al*., 2014). TCO is derived from the GMI simulation by integrating the generated ozone profiles from the surface up to tropopause pressure. GMI TCO (discussed below) was also averaged monthly and re-gridded from original 0.5^{o} latitude × 0.625^{o} longitude resolution to this same 5^{o} × 5^{o} gridding. Where we refer to GMI in this paper it is equivalent to MERRA-2 GMI.

2.3. Ozonesondes.

We include balloon-launched ozonesonde measurements for comparisons and validation of the OMI/MLS TCO. The ozonesonde database extends from 2004-2016 and includes measurements from Southern Hemisphere ADditional OZonesondes (SHADOZ) (Thompson et al., 2017; Witte et al., 2017), World Ozone and Ultraviolet Data Center (WOUDC) (https://woudc.org/), and

Atmos. Chem. Phys. Discuss., https://doi.org/10.5194/acp-2018-716
Manuscript under review for journal Atmos. Chem. Phys.
Discussion started: 5 December 2018

Network for the Detection of Atmospheric Composition Change (NDACC). (http://www.ndsc.ncep.noaa.gov/). The ozonesondes provide daily ozone profile concentrations as a function of altitude from several dozen global station sites. The ozone profiles are integrated vertically each day to derive tropospheric column measurements. Most all of the sonde ozone profile measurements are derived from Electrochemical Concentration Cell (ECC) instruments. The Supporting Material section discusses the ozonesonde analyses that include evaluation of potential offset and/or drift in OMI/MLS data.

2.4. Trend Calculations.

TCO offset differences between TOMS and OMI/MLS measurements are found to be regionally varying with offset difference values up to 5 DU or greater which hampers any useful effort for deriving trends from their concatenated datasets. Offsets of several DU between TOMS and OMI total ozone have been well documented (e.g., Witte et al., 2018, and references therein). Therefore, we have calculated trends independently for the TOMS (1979-2005) and OMI/MLS (2005-2016) datasets. Total net change in TCO (in DU) at each grid point for the 38-year record was determined by adding together the net changes (i.e. trend in DU-month^{-1} × number of months) for the TOMS and OMI/MLS records. Year 2017 and later months were not included in our analyses because the MERRA-2 GMI simulation ended after 2016 and also that the global ozonesonde measurements used for validating the OMI/MLS TCO extended only into mid-2016.

Multivariate linear regression (MLR) (Ziemke et al., 1997, and references therein) was applied to estimate trends in TCO. The regression includes components for the seasonal cycle, linear trend, and ENSO (e.g., Nino 3.4 index) from $TCO(x,t) = A(x,t) + B(x,t)\cdot t + C(x,t)\cdot Nino3.4(t) + \varepsilon(x,t)$, where x is the grid point and t is month. The term $\varepsilon(x,t)$ represents residual error. We applied two approaches regarding *Nino3.4*(t) in the MLR model. One approach was to de-trend *Nino*3.4(t) prior to the regression analysis and the other was not to de-trend this proxy. A main reason for possibly wanting to de-trend *Nino3.4*(t) is that TCO variability is not truly linear with *Nino3.4*(t) variability over any timescale including decadal which may potentially influence linear trend calculations in the MLR method. We opted not to include de-trending of *Nino3.4*(t) after finding little or no difference between either approach for both OMI/MLS and TOMS records. The seasonal coefficient A in the MLR equation above includes a constant plus annual and semi-annual harmonics while coefficients B and C each include a constant. Since our study does not evaluate seasonality of trends, we constrained the number of regression constants for trend B to only one which tends to improve overall trend statistical uncertainties when compared to using several regression seasonal constants for B. Trend magnitudes exceeding the calculated 2σ value uncertainty for B are deemed statistically significant. Calculated 2σ uncertainties for trends included an autoregressive-1 adjustment as presented in Weatherhead et al. (1998). Trends were calculated similarly for GMI TCO and NO emissions using this MLR approach.

3. Trends in Tropospheric Ozone.

3.1. The Aura Record (2005-2016).

OMI/MLS TCO trends for 60°S - 60°N are shown in Figure 1a with asterisks denoting regions that are statistically significant at 2σ level. Positive trends lie in the tropics and extra-tropics in both hemispheres with the largest trends (shown in red) of ~+3 DU-decade^{-1} or greater extending from India to East/SE Asia and further eastward over the Pacific Ocean. There are also statistically significant increases in ozone in the north Atlantic and Africa.

Trends for GMI TCO (Figure 1b) have several features similar to trends for OMI/MLS TCO. Large positive trends for GMI also extend from Saudi Arabia and India to SE/East Asia and further eastward over the Pacific Ocean. Changes for both OMI/MLS and GMI TCO over this region are ~+3 DU-decade^{-1}. GMI and OMI/MLS TCO also indicate positive trends extending from the tropical/subtropical Atlantic to Africa. There are clear differences between GMI and OMI/MLS in Figure 1, such as in the SH where GMI does not indicate statistically significant positive trends as the satellite observations do. Anet et al. (2017) examined surface ozone data from El Tololo, Chile (30°S, 71°W) and found a small positive trend of ~+0.7 ppbv-decade^{-1} for the period 1995-2010. Their analyses indicated that the positive increase at the site was driven mainly by stratospheric intrusions and not photochemical production from anthropogenic and biogenic precursors. The results from Anet et al. (2017) suggest that the positive trends in SH

OMI/MLS TCO in Figure 1a (primarily over ocean) may be real; however, one cannot make any conclusion based on only ground-level measurements and from only one station.

We have calculated ozonesonde column ozone trends for the same 2005-2016 Aura record to compare with the GMI and OMI/MLS TCO trends in Figure 1. (The Supporting Material discusses these trend comparisons.) Figure S10 of the Supporting Material indicates that it is not possible from the ozonesondes to conclude anything definitive regarding trends, particularly in the SH extra-tropics where the ozonesondes are relatively scarce over the short Aura time record.

Trends for NO emissions for 2005-2016 from the GMI simulation are shown in Figure 2, again with positive (negative) trends as red (blue). Largest increases in tropospheric NO in Figure 2 are located over India and east/SE Asia while greatest decreases originate over the eastern US, Europe, and Japan. We note that although there are large increases in NO emissions over eastern China for 2005-2016 depicted in Figure 2, observations show NO_2 decreased over this region after year 2012 (e.g., Krotkov et al., 2016). This recent downturn is not included in the GMI emissions, likely contributing to the overestimate of the ozone trend over eastern China in the GMI simulation. Overall, however, the ability of the GMI simulation to capture the positive trends above and downwind of regions with large NO_x emission increases suggests that the NO_x emission trends are driving the trends in TCO over India and east Asia.

Figure 1 shows that the regions of large decrease in NO such as the eastern US and Europe in Figure 2 do not coincide with similar decrease in TCO for either GMI or OMI/MLS. Both GMI and OMI/MLS TCO instead show essentially zero or slightly positive trends for these regions, despite the fact that the GMI simulation indicates significant negative trends in tropospheric column NO_2 over the eastern U.S. and Europe. This contrasts with the situation at the surface, in which simulations with GMI chemistry indicate decreases in surface ozone over the eastern U.S. in response to NO_x reductions (Strode et al., 2015).

Figure 3 shows comparisons between OMI/MLS and GMI deseasonalized TCO time series and their calculated linear trends for (a) SE Asia, (b) equatorial Africa, (c) NE Pacific, and (d) north Atlantic. Included in each panel are MLR regression fits for linear trends and their calculated 2σ uncertainties (both in DU-decade^{-1}). Not only are trends for GMI and OMI/MLS comparable and statistically significant in Figure 3 in each panel, but their month-to-month variations in their de-trended time series have relatively large cross-correlations varying from +0.64 to +0.70. Several inter-annual features are common with both MERRA-2 GMI and OMI/MLS TCO time series in Figure 3 such as large reductions (exceeding -5 DU) during spring 2008 over the NE Pacific and spring 2010 in the north Atlantic.

3.2. The TOMS Record (1979-2005).

Trends for TOMS (1979-2005) and GMI (1980-2005) TCO are shown in Figure 4. As with both OMI/MLS and GMI TCO for the Aura period 2005-2016 in Figure 1, largest positive trends in Figure 4 are also located over the Near East to East Asia and extending further eastward over the Pacific Ocean. Calculated trends for this region are ~+1.2 to +1.4 DU-decade^{-1} for both TOMS and GMI which are considerably smaller than during the Aura record. An important conclusion is that both the model and measurements in Figures 1 and 4 suggest that the trends in tropospheric ozone over this region are markedly larger during the Aura period compared to the earlier TOMS period, by a factor of about 2-2.5.

As with OMI/MLS and GMI TCO trends in Figure 1 there are discrepancies between the TOMS and model TCO trends in Figure 4. For TOMS TCO in Figure 4 there are regions of negative trends (in blue) as much as -0.6 DU-decade^{-1} over ocean in both hemispheres that are not explainable. Trends for GMI in Figure 4 are instead largely positive within these regions and actually positive throughout much of the SH when compared with TOMS. This suggests that the TOMS trends may be biased slightly low overall, provided that the simulation is closer to truth.

The trends for GMI TCO are positive over Brazil whereas OMI/MLS TCO shows only a hint of positive trends. It is likely that there will be smaller trends for TOMS because most ozone produced from biomass burning over Brazil lies in the low troposphere, and also that TOMS has reduced ability to detect ozone in the low troposphere. The GMI simulation shows that of the ~+1.4 DU-decade^{-1} TCO trend over Brazil in Figure 4, about +0.9 DU-decade^{-1} of this trend comes from ozone in the low troposphere below 500 hPa. With a known retrieval efficiency of

50-60% below 500 hPa (and essentially 100% above 500 hPa) for TOMS over Brazil, the model suggests that TOMS should detect a trend of about +0.5 DU-decade^{-1} below 500 hPa. Therefore TOMS would then have a trend in TCO of about +0.9 DU-decade^{-1} which is comparable to the ~+0.8 DU-decade^{-1} measured for TOMS in Figure 4.

In Figure 6 we show some examples of time series of TCO for TOMS and MERRA-2 GMI in regions where both records exhibit statistically significant positive trends. The positive correlations between TOMS and model TCO in Figure 6 are generally small compared to the correlations between OMI/MLS and model TCO in Figure 3. The only large correlation in Figure 6 is over Indonesia and is due to the intense El Nino of 1997-1998 that caused record increases in TCO in October 1997 in the region due to record levels of biomass burning (e.g., Chandra et al., 2003). The cross-correlations in the other panels in Figure 6 are small; these smaller correlations indicate the noisy nature of TOMS measurements compared to OMI/MLS and also possibly larger uncertainties present in meteorological winds, temperatures, and emissions during these earlier TOMS years for the GMI simulation.

A main result from Figures 4 and 6 is that the positive trends for both TOMS and MERRA-2 GMI TCO are substantially larger, by a factor of about 2 or more, during the OMI/MLS record compared to the TOMS record. The GMI simulation suggests that larger trends during the Aura record are the manifestation of an escalation of anthropogenic emissions and transport.

3.3. The Merged Record (1979-2016).

The net increases in tropospheric ozone over India and east/SE Asia for the merged 38-year record are sizable. Total changes in GMI and satellite-measured TCO for the merged record are shown in Figure 7 where contour values were determined by adding changes from the individual TOMS and OMI/MLS records together. There are two regions of greatest increase of TCO in Figure 7 for both GMI and the satellite measurements, one coinciding with the Near East to East Asia (increases of ~+6 to +7 DU, or about 15-20% average background ozone) and the other being tropical Africa/Atlantic (increases of ~+4 to +5 DU, of about 10-15% average background ozone). There is also an area of negative net change in the SH lying between Australia and the

Atmos. Chem. Phys. Discuss., https://doi.org/10.5194/acp-2018-716
Manuscript under review for journal Atmos. Chem. Phys.
Discussion started: 5 December 2018

maritime continent in Figure 7 for both GMI and measurements (shown in blue); these negative variations over the SH Indian Ocean appear small and are not statistically significant.

The color bar in Figure 7 also provides conversion from DU to tropospheric ozone mass surface density in units of metric tons per km^2. This conversion was included primarily to compare our results with the model simulation of Zhang et al. (2016). The large TCO trends over India and east/SE Asia in Figure 7 are about +0.13 to +0.15 metric tons per km^2 for both GMI and the satellite data. These numbers are comparable to increases of ~+0.11 metric tons per km^2 for this region as modeled by Zhang et al. (2016) for years 1980-2010.

Figure 8 shows TCO time series from the merged satellite measurements for 1979-2016 centered over the two regions of largest increase in Figure 7 (i.e., eastern Asia and equatorial Africa). In both panels TOMS is the solid red curve and OMI/MLS is the dotted blue curve. For plotting purposes, offsets were applied to the TOMS data in both panels using 2005 overlap measurements (see figure and caption). The last five years in both panels in Figure 8 shows that current OMPS TCO (solid black curves) with several years of overlap with OMI/MLS TCO will be useful to continue the OMI/MLS record which has already extended past 13 years.

Studies suggest that ozone in the lower stratosphere in both hemispheres has been decreasing over the last 1-2 decades despite the decrease in global CFCs following the 1987 Montreal Protocol. Ball et al. (2018) evaluated global ozone trends for 1985-2016 by combining models with measurements from several satellite instruments. A conjecture as stated by Ball et al. (2018) is that while ozone in the upper stratosphere above ~10 hPa appears to be recovering, ozone in the lower stratosphere appears to be decreasing which models do not seem to replicate despite the decrease in CFCs. A main point of Ball et al. (2018) is that total ozone has not changed because the ongoing stratospheric ozone decrease is opposed by tropospheric ozone increase. A global decrease in lower stratospheric ozone of about 2 DU below 32 hPa was detected by Ball et al. (2018) and it appeared to be compensated largely by opposite increases in tropospheric ozone. In their study they included OMI/MLS TCO for 2005-2016 (i.e., their Figure 4 and Figure S13) and measured a trend in 60°S-60°N TCO of about +1.7 DU-decade^{-1} which mostly cancels out the negative trend in stratospheric ozone. Wargan et al. (2018) in a

Atmos. Chem. Phys. Discuss., https://doi.org/10.5194/acp-2018-716
Manuscript under review for journal Atmos. Chem. Phys.
Discussion started: 5 December 2018

related paper evaluated MERRA-2 assimilated ozone for 1998-2016 using an idealized atmospheric tracer also driven from MERRA-2 meteorological fields. Similar to Ball et al. (2018), Wargan et al. (2018) also found net decrease in ozone in the lower stratosphere (i.e., within a 10 km layer above the tropopause) in both hemispheres; their trend values were about -1.2 DU-decade^{-1} in the SH and about -1.7 DU-decade^{-1} in the NH. Wargan et al. (2018) found evidence that these negative trends over the last two decades have been driven by enhanced isentropic transport of ozone between the tropical and extratropical lower stratosphere.

The increases in measured TCO from TOMS and OMI/MLS as indicated in Figures 1, 3, 4 and in Figures 6-8 can have implications for evaluating global ozone trends, particularly for trends in total column ozone and assessment of the recovery of stratospheric ozone. One should be careful using total ozone to infer stratosphere ozone recovery if trends in TCO are not accounted for. The increases in TCO of +6 to +7 DU in Figures 7-8 for India-eastern Asia represent a sizeable change even for total column ozone.

4. Summary.

Studies suggest that ozone in the troposphere has increased globally throughout much of the 20th century due largely to increases in anthropogenic emissions. We provide evidence from combined satellite measurements and a chemical transport model that tropospheric ozone over the last four decades does indeed indicate increases that are global in nature, yet highly regional due to combined effects of regional pollution and transport.

We have obtained tropospheric ozone trends for 1979-2016 by merging TOMS (1979-2005) and Aura OMI/MLS (2005-2016) satellite measurements. We included the MERRA-2 GMI CTM simulation to evaluate and possibly explain the global trend patterns found for both TOMS and OMI/MLS TCO. Trends were calculated independently for TOMS and OMI/MLS records using a linear regression model. Net changes in both measured and modeled TCO for the entire merged record were estimated by adding net changes for the TOMS and OMI/MLS time periods together.

A persistent trend pattern emerges with TCO for the GMI simulation and satellite measurements for both the TOMS and OMI/MLS records. The GMI model, and also measurements from TOMS and OMI/MLS all independently show large (positive) trends in TCO in the NH extending from the Near East to India and east/SE Asia, and further eastward over the Pacific Ocean. An important finding is that the trends in TCO for both the GMI model and satellite measurements for this region are smaller during the earlier part of the merged record; that is, the trends for both GMI and satellite measurements increase from about +1.2 to +1.4 DU-decade^{-1} (1979-2005) to about +3 DU-decade^{-1} or greater (2005-2016). Analysis of the NO emissions input to the GMI simulation indicates that the measured trends in tropospheric ozone in this region including the escalation of increased trends during the latter Aura period are consistent with increases in pollution in the region.

For the long merged record there are again strong similarities between the GMI simulation and satellite measurements of TCO. Net changes in tropospheric ozone for India and east/SE Asia for 1979-2016 are about +6 to +7 DU, or about 0.13-0.15 metric tons per km^2 for both the GMI and satellite TCO. These are pronounced increases in TCO representing ~15-20% average TCO background amounts. Both the GMI simulation and satellite measurements show that of these +6 to +7 DU increases over this broad area, about half or slightly most of the change (i.e., ~+4 DU) occurs during the Aura time record of 2005-2016. The GMI simulation and satellite measurements also depict a secondary maximum of TCO increase for 1979-2016 over the tropical Atlantic/Africa region of about +4 to +5 DU (~10-15% average background ozone).

Acknowledgments. We thank the NASA Goddard Space Flight Center Ozone Processing Team for the TOMS and OMI total ozone measurements and the Jet Propulsion Laboratory MLS team for MLS v4.2 ozone. OMI is a Dutch-Finnish contribution to the Aura mission. We also thank WOUDC and the NDACC for providing extensive ozonesonde measurements that we used for the comparisons/validation of satellite tropospheric ozone. Funding for this research was provided in part by NASA NNH14ZDA001N-DSCOVR. We also thank the NASA MAP program for supporting the MERRA-2 GMI simulation and the NASA Center for Climate Simulation (NCCS) for providing high-performance computing resources. More information on the MERRA-2 GMI simulation and access is available at https://acd-

ext.gsfc.nasa.gov/Projects/GEOSCCM/MERRA2GMI/. Tropospheric ozone data used in this study are available from NASA Goddard Space Flight Center at http://acdb-ext.gsfc.nasa.gov/Data_services/cloud_slice/ and links from the Aura Validation Data Center (https://avdc.gsfc.nasa.gov/).

References.

Allen, D., K. Pickering, B. Duncan, and M. Damon, Impact of lightning NO emissions on North American photochemistry as determined using the Global Modeling Initiative (GMI) model, J. Geophys. Res., Atmos., 115(D22301), doi:10.1029/2010JD014062, 2010.

Anet, J. G., M. Steinbacher, L. Gallardo, P. A. Velasquez Alvarez, L. Emmenegger, and B. Buchmann, Surface ozone in the Southern Hemisphere: 20 years of data from a site with a unique setting in El Tololo, Chile, Atmos. Chem. Phys., 17, 6477–6492, doi:10.5194/acp-17-6477-2017, 2017.

Ball, W.T., J. Alsing, J. Staehelin, T. Peter, D. J. Mortlock, J. D. Haigh, F. Tummon, R. Stubli, A. Stenke, J. Anderson, A. Bourassa, S. Davis, D. Degenstein, S. Frith, L. Froidevaux, G. Labow, C. Roth, V. Sofieva, R. Wang, J. Wild, J. Ziemke, E. V. Rozanov, Continuous decline in lower stratospheric ozone offsets ozone layer recovery, Atmos. Chem. Phys., 18, 1379-1394, https://doi.org/10.5194/acp-18-1379-2018, 2018.

Beig, G., and V. Singh, Trends in tropical tropospheric column ozone from satellite data and MOZART model, Geophys. Res. Lett., 34, L17801, doi:10.1029/2007GL030460, 2007.

Bulletin of the American Meteorological Society State of the Climate Report, 2017.

Cecil, D. J., D. E. Buechler, and R. J. Blakeslee, Gridded lightning climatology fromTRMM-LIS and OTD: Dataset description, Atmos. Res., 135, 404-414, doi:10.1016/j.atmosres.2012.06.028, 2014.

Chandra S., J. R. Ziemke, and R. W. Stewart, An 11-year solar-cycle in tropospheric ozone from TOMS measurements, Geophys. Res. Lett., 26, 185-188, doi:10.1029/1998GL900272, 1999.

Chandra, S., J. R. Ziemke, and R. V. Martin, Tropospheric ozone at tropical and middle latitudes derived from TOMS/MLS residual: Comparison with a global model, J. Geophys. Res., 108(D9), 4291, doi:10.1029/2002JD002912, 2003.

Cooper, O. R., D. D. Parrish, J. R. Ziemke, N. V. Balashov, M. Cupeiro, I. Galbally, S. Gilge, L. Horowitz, N. R. Jensen, J.-F Lamarque, V. Naik, S. J. Oltmans, J. Schwab, D. T. Shindell, A. M. Thompson, V. Thouret, Y. Wang, and R. M. Zbinden, Global distribution and trends of tropospheric ozone: An observation-based review, Elementa: Science of the Anthropocne, 2, 000029, doi:10.12952/journal.elementa.000029, 2014.

Duncan, B. N., R. V. Martin, A. C. Staudt, R. Yevich, and J. A. Logan, Interannual and seasonal variability of biomass burning emissions constrained by satellite observations, Journal of Geophysical Research-Atmospheres, 108(D2), doi:10.1029/2002jd002378, 2003.

Duncan, B.N., S.E. Strahan, Y. Yoshida, S.D. Steenrod, and N. Livesey, Model study of cross-tropopause transport of biomass burning pollution, Atmos. Chem. Phys., 7, 3713-3736, doi:10.5194/acp-7-3713-2007, 2007.

Fioletov, V. E., G. J. Labow, R. Evans, E. W. Hare, U. Kohler, C. T. McElroy, K. Miyagawa, A. Redondas, V. Savastiouk, A. M. Shalamyansky, J. Staehelin, K. Vanicek, and M. Weber, Performance of the ground-based total ozone network assessed using satellite data, J. Geophys. Res., 113, D14313, doi:10.1029/2008JD009809, 2008.

Gaudel, A., O. R. Cooper, G. Ancellet, B. Barret, A. Boynard, J. P. Burrows, C. Clerbaux, P.-F. Coheur, J. Cuesta, E. Cuevas, S. Doniki, G. Dufour, F. Ebojie, G. Foret, O. Garcia, M. J. Granados-Muñoz, J. Hannigan, F. Hase, B. Hassler, G. Huang, D. Hurtmans, D. Jaffe, N. Jones, P. Kalabokas, B. Kerridge, S. Kulawik, B. Latter, T. Leblanc, E. Le Flochmoën, W. Lin, J. Liu, X. Liu, E. Mahieu, A. McClure-Begley, J. Neu, M. Osman, M. Palm, H. Petetin, I.

Petropavlovskikh, R. Querel, N. Rahpoe, A. Rozanov, M. G. Schultz, J. Schwab, R. Siddans, D. Smale, M. Steinbacher, H. Tanimoto, D. Tarasick, V. Thouret, A. M. Thompson, T. Trickl, E. Weatherhead, C. Wespes, H. Worden, C. Vigouroux, X. Xu, G. Zeng, J. Ziemke, Tropospheric Ozone Assessment Report: Present-day distribution and and trends of tropospheric ozone relevant to climate and global atmospheric chemistry model evaluation, Elem Sci Anth, 6(39), https://doi.org/10.1525/elementa.291, 2018.

Gelaro, R., W. McCarty, M.J. Suárez, R. Todling, A. Molod, L. Takacs, C.A. Randles, A. Darmenov, M.G. Bosilovich, R. Reichle, K. Wargan, L. Coy, R. Cullather, C. Draper, S. Akella, V. Buchard, A. Conaty, A.M. da Silva, W. Gu, G. Kim, R. Koster, R. Lucchesi, D. Merkova, J.E. Nielsen, G. Partyka, S. Pawson, W. Putman, M. Rienecker, S.D. Schubert, M. Sienkiewicz, and B. Zhao, The Modern-Era Retrospective Analysis for Research and Applications, Version 2 (MERRA-2), J. Climate, 30, 5419–5454, https://doi.org/10.1175/JCLI-D-16-0758.1, 2017.

Giglio, L., J. Randerson, and G. van der Werf, Analysis of daily, monthly, and annual burned area using the fourth-generation global fire emissions database (GFED4), Journal of Geophysical Research-Biogeosciences, 118(1), 317-328, doi:10.1002/jgrg.20042, 2013.

Granier, C., B. Bessagnet, T. Bond, A. D'Angiola, H. D. van der Gon, et al., Evolution of anthropogenic and biomass burning emissions of air pollutants at global and regional scales during the 1980–2010 period. Climatic Change, 109, 163–190, doi:10.1007/s10584-011-0154-1, 2011.

Heue, K.-P., M. Coldewey-Egbers, A. Delcloo, C. Lerot, D. Loyola, P. Valks, and M. van Roozendael, Trends of tropical tropospheric ozone from 20 years of European satellite measurements and perspectives for the Sentinel-5 Precursor, Atmos. Meas. Tech., 9, 5037-5051, https://doi.org/10.5194/amt-9-5037-2016/, 2016.

Krotkov, N. A., C. A. McLinden, C. Li,, L. N. Lamsal, E. A. Celarier, S. V. Marchenko, William H. Swartz, Eric J. Bucsela, Joanna Joiner, Bryan N. Duncan, K. Folkert Boersma, J. Pepijn Veefkind, Pieternel F. Levelt, Vitali E. Fioletov, Russell R. Dickerson, Hao He, Zifeng Lu, and

David G. Streets, Aura OMI observations of regional SO2 and NO2 pollution changes from 2005 to 2015, Atmos. Chem. Phys., 16, 4605–4629, doi:10.5194/acp-16-4605-2016, 2016.

Lamarque, J.-F., T. C. Bond, V. Eyring, C. Granier, A. Heil, Z. Klimont, D. Lee, C. Liousse, A. Mieville, B. Owen, M. G. Schultz, D. Shindell, S. J. Smith, E. Stehfest, J. Van Aardenne, O. R. Cooper, M. Kainuma, N. Mahowald, J. R. McConnell, V. Naik, K. Riahi, and D. P. van Vuuren, Historical (1850-2000) gridded anthropogenic and biomass burning emissions of reactive gases and aerosols: methodology and application, Atmospheric Chemistry and Physics, 10(15), 7017-7039, doi:10.5194/acp-10-7017-2010, 2010.

Lee H. -J., S. -W. Kim, J. Brioude, O. R. Cooper, G. J. Frost, C. –H. Kim, R. J. Park, M. Trainer, and J. –H. Woo, Transport of NO_x in East Asia identified by satellite and in-situ measurements and Lagrangian particle dispersion model simulations. J. Geophys. Res., 119, 2574–2596, doi:10.1002/2013JD021185, 2014.

Leventidou, E. K., U. Eichmann, M. Weber, and J. P. Burrows, Tropical tropospheric ozone columns from nadir retrievals of GOME-1/ERS2, SCIEMACHY/Envisat, and GOME-2/MetOp-A (1996-2012), Atmos. Meas. Tech., 9, 3407-3427, doi:10.5194/amt-9-3407-2016, 2016.

Leventidou, E., M. Weber, K.-U. Eichmann, J. P. Burrows, K.-P. Heue, A. M. Thompson, and B. J. Johnson, Harmonization and trends of 20-years tropical tropospheric ozone data, Atmos. Chem. Phys. Discuss., 18, 9189-9205, https://doi.org/10.5194/acp-18-9189-2018, 2018.

Lin, M., L. W. Horowitz, R. Payton, A. M. Fiore, and G. Tonnesen, US surface ozone trends and extremes from 1980 to 2014: Quantifying the roles of rising Asian emissions, domestic controls, wildfires, and climate, Atmos. Chem. Phys., 17, 2943–2970, doi:10.5194/acp-17-2943-2017, 2017.

McPeters, R. D., S. M. Frith, N. A. Kramarova, J. R. Ziemke, and G. L. Labow, OMI total column ozone: Extending the long-term data record (2018), Trend Quality Ozone from NPP OMPS: the Version 2 Processing, Atmos. Meas. Tech., doi:amt-2018-209, 2018, 2017.

Molod, A., L. Takacs, M. Suarez, and J. Bacmeister, Development of the GEOS-5 atmospheric general circulation model: evolution from MERRA to MERRA2, Geosci Model Dev., 8, doi:10.5194/gmd-8-1339-2015, 2015.

Nielsen, J. E., S. Pawson, A. Molod, B. Auer, A. M da Silva, A. R. Douglass, B. Duncan, Q. Liang, M. Manyin, L. D. Oman, W. Putman, S. E. Strahan, K. Wargan, Chemical mechanisms and their applications in the Goddard Earth Observing System (GEOS) earth system model. Journal of Advances in Modeling Earth Systems, 9, 3019–3044. https://doi.org/10.1002/2017MS001011, 2017.

Oman, L. D., A. R. Douglass, J. R. Ziemke, J. M. Rodriguez, D. W. Waugh, and J. E. Nielsen, The ozone response to ENSO in Aura satellite measurements and a chemistry-climate simulation, J. Geophys. Res., 118, 965-976, doi:10.1029/2012JD018546, 2013.

Orbe, C., L. D. Oman, S. E. Strahan, D. W. Waugh, S. Pawson, L. L. Takacs, and A. M. Molod, Large-Scale Atmospheric Transport in GEOS Replay Simulations. Journal of Advances in Modeling Earth Systems 9, 2545-2560, 2017.

Parrish, D. D., K. S. Law, J. Staehelin, R. Derwent, O. R. Cooper, H. Tanimoto, Volz-Thomas, S. Gilge, H.-E. Scheel, M. Steinbacher, and E. Chan, Lower tropospheric ozone at northern mid-latitudes: Changing seasonal cycle. Geophys. Res. Lett, 40, 1631–1636. doi:10.1002/grl.50303, 2013.

Shepherd, T. G., D. A. Plummer, J. F. Scinocca, M. I. Hegglin, V. E. Fioletov, M. C. Reader, E. Remsberg, T. von Clarmann, and H. J. Wang, Reconciliation of halogen-induced ozone loss with the total-column ozone record, Nature Geosci., 7, doi:10.1038/NGEO2155, 2014.

Strode, S. A., J. M. Rodriguez, J. A. Logan, O. R. Cooper, J. C. Witte, L. N. Lamsal, M. Damon, B. Van Aartsen, S. D. Steenrod, and S. E. Strahan, Trends and variability in surface ozone over the United States, Journal of Geophysical Research-Atmospheres, 120(17), 9020-9042, doi:10.1002/2014JD022784, 2015.

Thompson, A. M., and R. D. Hudson, Tropical tropospheric ozone (TTO) maps from Nimbus 7 and Earth Probe TOMS by the modified residual method: Evaluation with sondes, ENSO signals, and trends from Atlantic regional time series, J. Geophys. Res., 104(D21), 26,961-26,975, doi:10.1029/1999JD900470, 1999.

Thompson, A. M., J. C. Witte, C. Sterling, A. Jordan, B. J. Johnson, S. J. Oltmans, M. Fujiwara, H. Vömel, M. Allaart, A. Piters, G. J. R. Coetzee, F. Posny, E. Corrales, J. Andres Diaz, C. Félix, N. Komala, N. Lai, M. Maata, F. Mani, Z. Zainal, S-Y. Ogino, F. Paredes, T. Luiz Bezerra Penha, F. Raimundo da Silva, S. Sallons-Mitro, H. B. Selkirk, F. J. Schmidlin, R. Stuebi, K. Thiongo, First reprocessing of Southern Hemisphere Additional Ozonesondes (SHADOZ) Ozone Profiles (1998-2016). 2. Comparisons with satellites and ground-based instruments, J. Geophys. Res., 122, 13000-13025, doi: 10.1002/2017 JD027406, 2017.

Vasilkov, A., J. Joiner, R. Spurr, P. K. Bhartia, P. Levelt, and G. Stephens, Evaluation of the OMI cloud pressures derived from rotational Raman scattering by comparisons with other satellite data and radiative transfer simulations, J. Geophys. Res., 113, D15S19, doi:10.1029/2007JD008689, 2008.

Wargan, K., C. Orbe, S. Pawson, J. R. Ziemke, L. D. Oman, M. A. Olsen, L. Coy, K. E. Knowland, Recent decline in lower stratospheric ozone attributed to circulation changes, GRL, Geophys. Res. Lett., 45, 5166-5176, https://doi.org/10.1029/2018GL077406, 2018.

Weatherhead, E. C., G. C. Reinsel, G. C. Tiao, X.-L Meng, D. Choi, W-K Cheang, T. Keller, J. DeLuisi, D. J. Wuebbles, J. B. Kerr, A. J. Miller, Samuel J. Oltmans, John E. Frederick, Factors affecting the detection of trends: Statistical considerations and applications to environmental data, 17149–17161, 103(D14), doi:10.1029/98JD00995, 1998.

Atmos. Chem. Phys. Discuss., https://doi.org/10.5194/acp-2018-716
Manuscript under review for journal Atmos. Chem. Phys.
Discussion started: 5 December 2018

Wespes, C., D. Hurtmans, C. Clerbaux, and P.-F. Coheur, O3 variability in the troposphere as observed by IASI over 2008–2016: Contribution of atmospheric chemistry and dynamics, J. Geophys. Res. Atmos., 122, 2429–2451, doi:10.1002/2016JD025875, 2017.

Witte J. C., A. M. Thompson, H. G. J. Smit, M. Fujiwara, F. Posny, G. J. R. Coetzee, E. T. Northam, B. J. Johnson, C. W. Sterling, M. Mohammed, S-Y. Ogino, A. Jordan, F. Raimundo daSilva, Z. Zainal, First reprocessing of Southern Hemisphere ADditional OZonesondes (SHADOZ) profile records (1998-2015) 1: Methodology and evaluation, J. Geophys. Res., 122, 6611-6636, doi:10.1002/2016JD026403, 2017.

Witte, J. C., A. M. Thompson, H. G. J. Smit, H. Vömel, F. Posny, R. Stuebi, First reprocessing of Southern Hemisphere Additional Ozonesondes (SHADOZ) Profile Records. 3. Uncertainty in ozone profile and total column, J. Geophys. Res., 123, doi:10.1002/2017JD027791, 2018.

Wolf, F. L., Elements of Probability and Statistics, McGraw-Hill, New York, 1962.

Yienger, J. J., and H. Levy, Empirical-model of global soil-biogenic NOx emissions, Journal of Geophysical Research-Atmospheres, 100(D6), 11447-11464, doi:10.1029/95jd00370, 1995.

Zhang, Y., O. R. Cooper, A. Gaudel, A. M. Thompson, P. Nedelec, S.-Y. Ogino, and J. J. West, Tropospheric ozone change from 1980 to 2010 dominated by equatorward re-distribution of emissions, Nature Geosci. 9, 875-879, doi:10.1038/NGEO2827, 2016.

Ziemke, J. R., S. Chandra, and P. K. Bhartia, Two new methods for deriving tropospheric column ozone from TOMS measurements: The assimilated UARS MLS/HALOE and convective-cloud differential techniques, J. Geophys. Res., 103, 22,115-22,127, 1998.

Ziemke, J. R., S. Chandra, and P. K. Bhartia, A 25-year data record of atmospheric ozone from TOMS Cloud Slicing: Implications for trends in stratospheric and tropospheric ozone, J. Geophys. Res., 110, D15105, doi:10.1029/2004JD005687, 2005.

Ziemke, J. R., S. Chandra, B. N. Duncan, L. Froidevaux, P. K. Bhartia, P. F. Levelt, and J. W. Waters, Tropospheric ozone determined from Aura OMI and MLS: Evaluation of measurements and comparison with the Global Modeling Initiative's Chemical Transport Model, J. Geophys. Res., 111, D19303, doi:10.1029/2006JD007089, 2006.

Ziemke, J. R., J. Joiner, S. Chandra, P. K. Bhartia, A. Vasilkov, D. P. Haffner, K. Yang, M. R. Schoeberl, L. Froidevaux, and P. F. Levelt, Ozone mixing ratios inside tropical deep convective clouds from OMI satellite measurements, Atmos. Chem. Phys., 9, 573-583, 2009.

Ziemke, J. R., and S. Chandra, Development of a climate record of tropospheric and stratospheric ozone from satellite remote sensing: Evidence of an early recovery of global stratospheric ozone, Atmos. Chem. Phys., 12, 5737-5753, doi:10.5194/acp-12-5737-2012, 2012.

Ziemke, J. R., A. R. Douglass, L. D. Oman, S. E. Strahan, and B. N. Duncan, Tropospheric ozone variability in the tropical Pacific from ENSO to MJO and shorter timescales, Atmos. Chem. Phys., 15, 8037-8049, doi:10.5194/acp-15-8037-2015, 2015.

Ziemke, J. R., and O. R. Cooper, Tropospheric ozone, in State of the Climate Report for 2016, Bull. Amer. Meteorol., 2018.

FIGURES AND FIGURE CAPTIONS

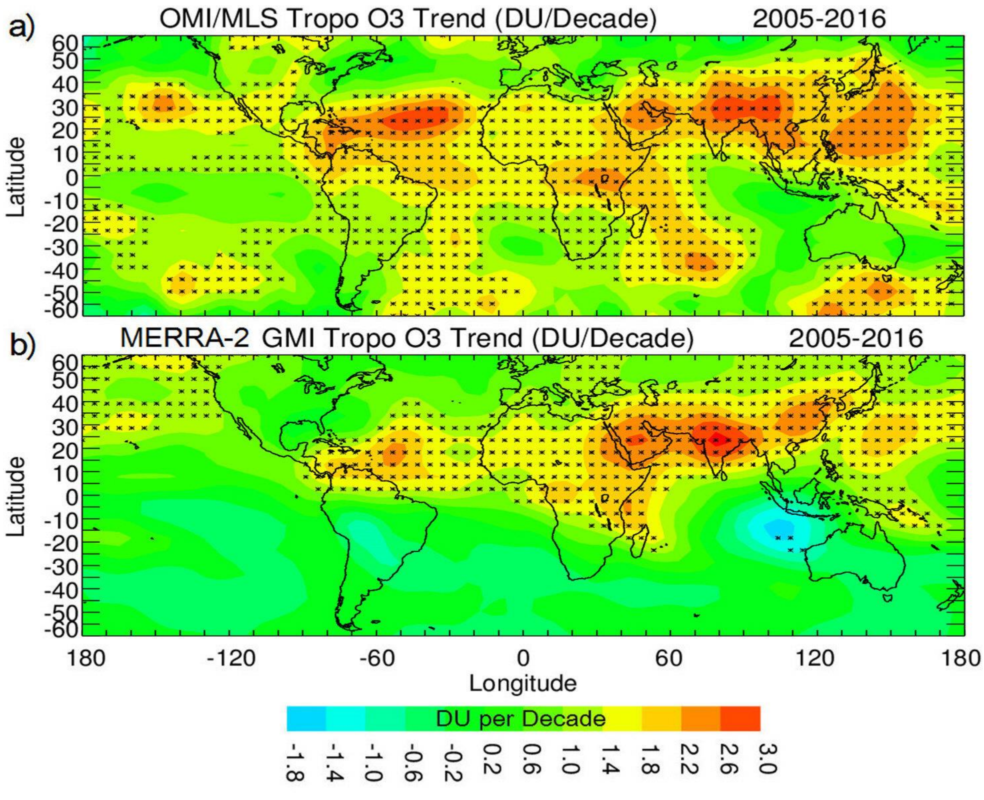

Figure 1. (a) Trends in OMI/MLS TCO (in DU-decade^{-1}) for 2005-2016. Asterisks denote grid points where trends are statistically significant at the 2σ level. (b) Same as (a) except for MERRA-2 GMI TCO.

Atmos. Chem. Phys. Discuss., https://doi.org/10.5194/acp-2018-716
Manuscript under review for journal Atmos. Chem. Phys.
Discussion started: 5 December 2018

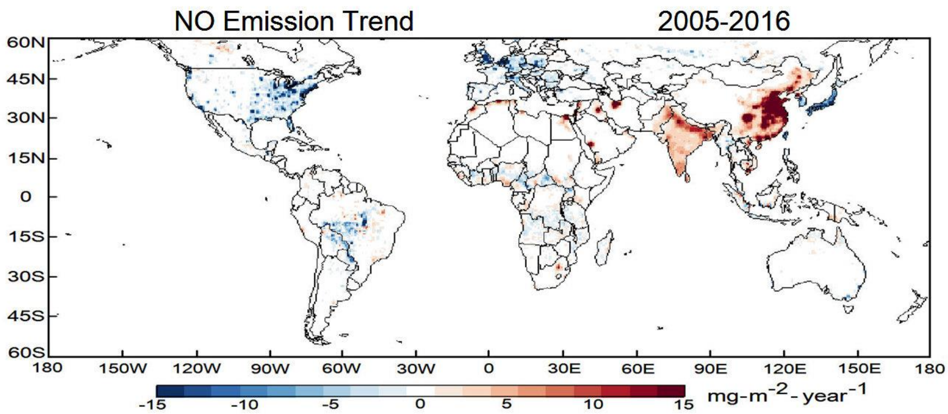

Figure 2. Trends in MERRA-2 GMI NO emissions (units mg-m $^{-2}$-y^{-1}) for 2005-2016.

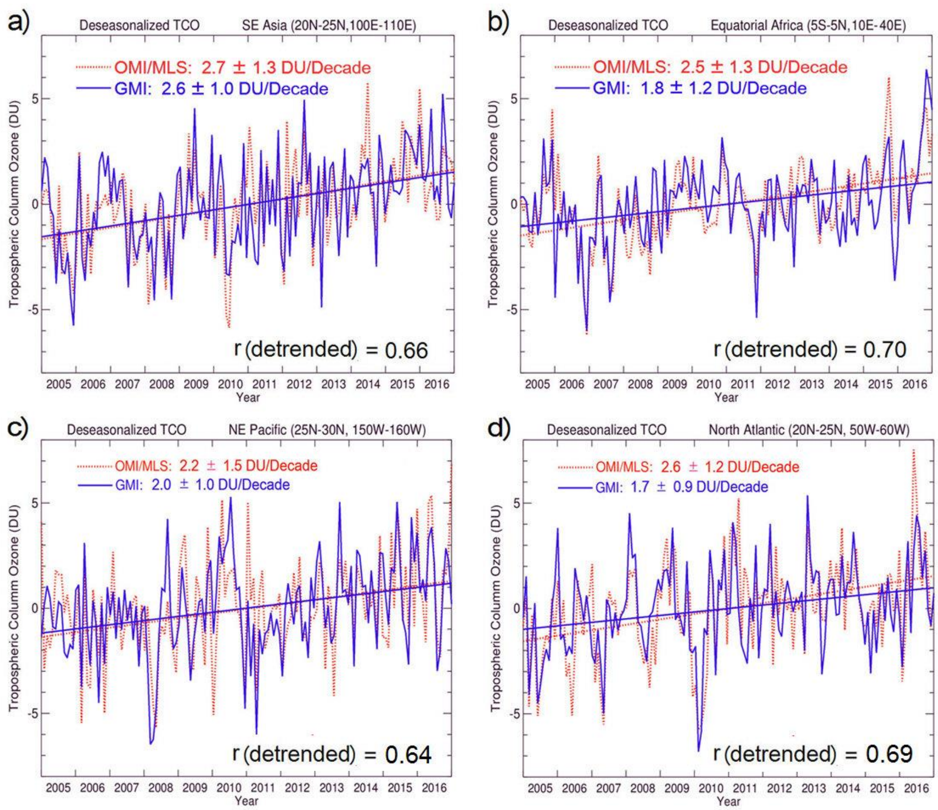

Figure 3. (a) Deseasonalized TCO for OMI/MLS (red, dashed curve) and the MERRA-2 GMI model (blue, solid curve) for SE Asia. Included are MLR regression fits for linear trends and calculated 2σ values (both in DU-decade^{-1}). Shown at the bottom is the correlation r between the two time series after removing their linear trends. (b) Same as (a), but for equatorial Africa. (c) Same, but for NE Pacific. (d) Same, but for north Atlantic.

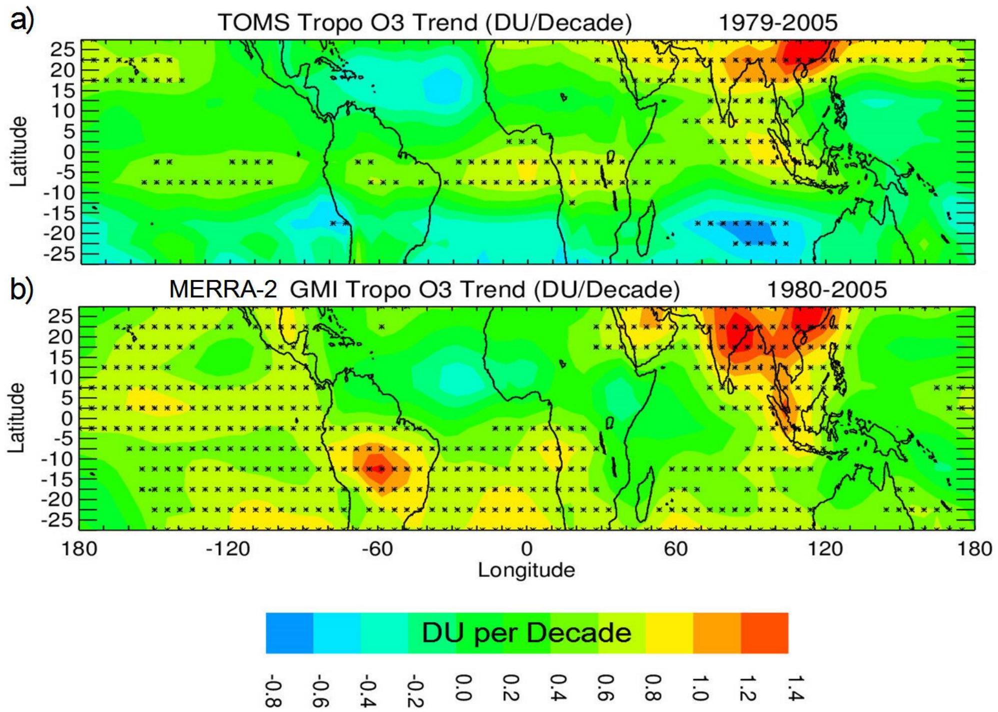

Figure 4. (top) Trends (DU-decade^{-1}) calculated for TOMS CCD TCO measurements for years 1979-2005. Asterisks denote grid points where trends are statistically significant at the 2σ level. (bottom) Similar to (top), but for MERRA-2 GMI TCO and for 1980-2005.

Atmos. Chem. Phys. Discuss., https://doi.org/10.5194/acp-2018-716
Manuscript under review for journal Atmos. Chem. Phys.
Discussion started: 5 December 2018

Atmospheric Chemistry and Physics
Discussions

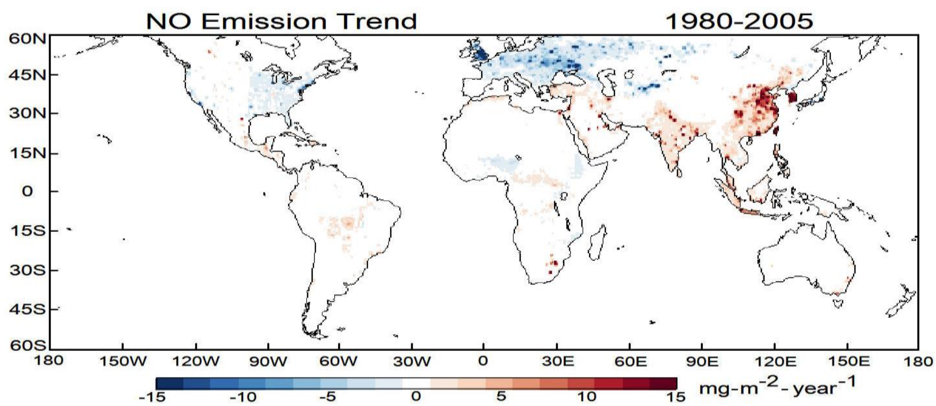

Figure 5. Trends in MERRA-2 GMI NO emissions (units mg-m $^{-2}$-y^{-1}) from biomass burning for 1980-2005.

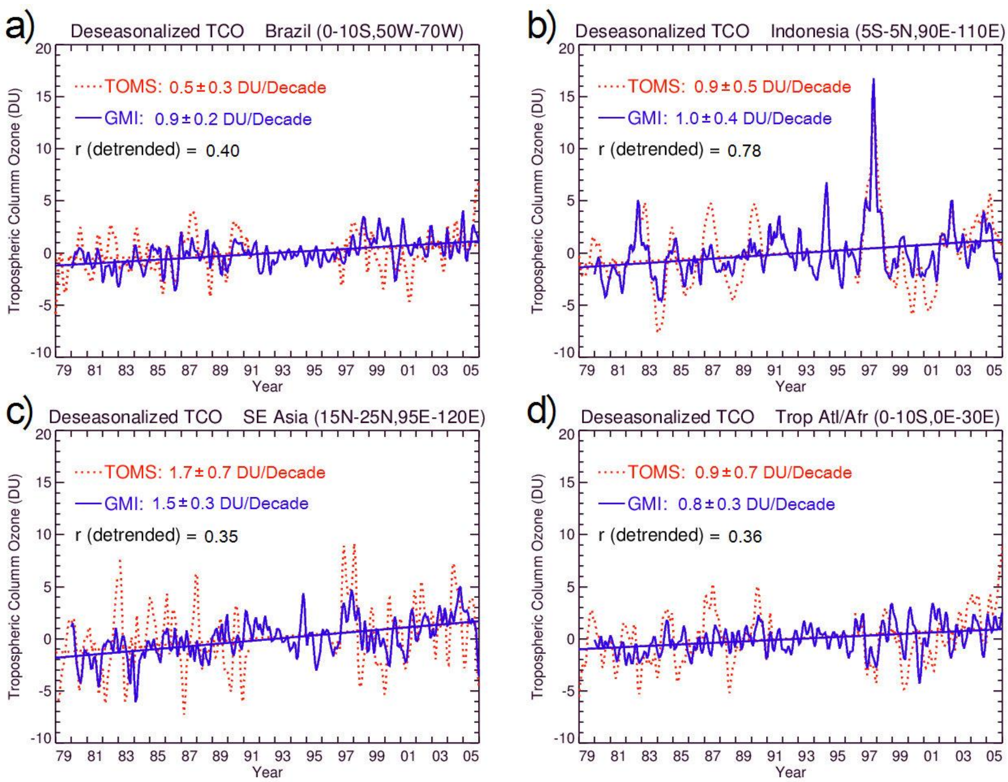

Atmos. Chem. Phys. Discuss., https://doi.org/10.5194/acp-2018-716
Manuscript under review for journal Atmos. Chem. Phys.
Discussion started: 5 December 2018

Figure 6. (a) Deseasonalized TCO for TOMS (red, dashed curve) and the MERRA-2 GMI model (blue, solid curve) for Brazil. Included are their MLR linear trends and calculated 2σ values (both in DU-decade^{-1}) averaged over the specified region. Shown also is the cross-correlation r between the two time series after removing their linear trends. (b) Same as (a), but for Indonesia. (c) Same as (a) but for SE Asia. (d) Same as (a) but for tropical Atlantic/Africa.

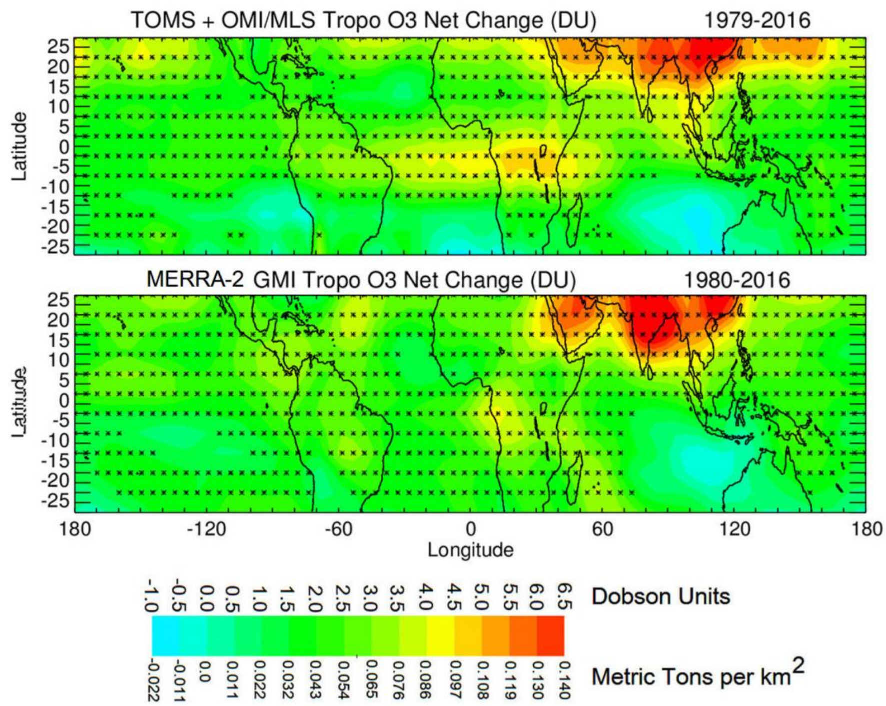

Figure 7. (top) Net changes in TOMS and OMI/MLS TCO calculated for their combined time records (1979-2016). The net changes for TCO are shown in the color bar in both DU and metric tons of ozone per km^2 (1 DU ≡ 0.0214 metric tons per km^2 for ozone). Asterisks denote grid points where net changes are statistically significant at the 2σ noise level. (bottom) Similar to (top), but for GMI TCO and years 1980-2016. Net change for GMI TCO is determined similar to the satellite measurements by adding together the net changes for the two records (i.e., for GMI, the 1980-2005 and 2005-2016 periods).

Atmos. Chem. Phys. Discuss., https://doi.org/10.5194/acp-2018-716
Manuscript under review for journal Atmos. Chem. Phys.
Discussion started: 5 December 2018

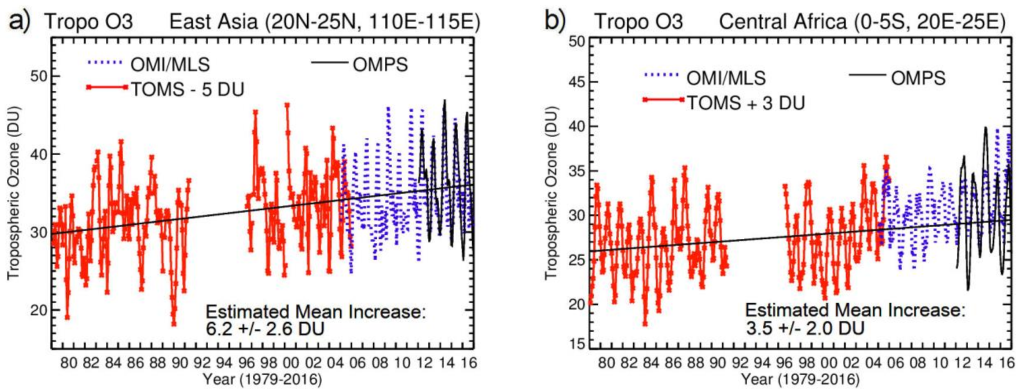

Figure 8. (a) Merged time series of TOMS/OMI/MLS/OMPS TCO for 1979-2016 over east Asia centered at 22.5° N and 112.5° E (5° × 5° region). The solid red curve is TOMS TCO and dashed blue curve is OMI/MLS. OMPS TCO (solid black curve) is also over-plotted with OMI/MLS TCO starting 2012 for comparison. A constant adjustment of about -5 DU (using year 2005 coincident overlap data) was applied to the TOMS measurements for plotting with OMI/MLS. Both OMI/MLS and OMPS TCO also included offsets of +2 DU and -2 DU following comparisons with ozonesonde measurements (see Supplementary Material). The indicated total increase of 6.2 DU was estimated using a regression best-fit line (black line shown) to the TOMS/OMI/MLS merged time series and agrees well with the 6-7 DU net increase for this region in Figure 7. (b) Similar to (a) except for central Africa centered at 2.5° S, 22.5° E and a TOMS offset of +3 DU. The line-fit increase is slightly smaller than the 4-5 DU in Figure 7. The estimated mean increases in both panels include calculated 2σ uncertainties.